Depleted-heterojunction colloidal quantum dot photovoltaics employing low-cost electrical contacts

Ratan Debnath,[1] Mark T. Greiner,[2] Illan J. Kramer,[1] Armin Fischer,[1] Jiang Tang,[2] D. Aaron R. Barkhouse,[1] Xihua Wang,[1] Larissa Levina,[1] Zheng-Hong Lu,[2,3] and Edward H. Sargent[1,a)]

[1]*Department of Electrical and Computer Engineering, University of Toronto, 10 King's College Road, Toronto, Ontario M5S 3G4, Canada*
[2]*Department of Materials Science and Engineering, 184 College Street, Toronto, Ontario M5S 3E4, Canada*
[3]*Department of Physics, Yunnan University, 2 Cuihu Beilu, Yunnan, Kunming 650091, People's Republic of China*

(Received 14 June 2010; accepted 16 June 2010; published online 15 July 2010)

With an aim to reduce the cost of depleted-heterojunction colloidal quantum dot solar cells, we describe herein a strategy that replaces costly Au with a low-cost Ni-based Ohmic contact. The resultant devices achieve 3.5% Air Mass 1.5 power conversion efficiency. Only by incorporating a 1.2-nm-thick LiF layer between the PbS quantum dot film and Ni, we were able to prevent undesired reactions and degradation at the metal-semiconductor interface. © *2010 American Institute of Physics*. [doi:10.1063/1.3463037]

Solar energy harvesting requires a combination of low cost and high efficiency to overcome balance-of-systems cost. Solution-processing offers an attractive route to low cost per area of light-harvesting material. Among solution-processed semiconductors, colloidal quantum dots offer the advantage of a widely-tunable band gap, providing both optimal-band gap solution-processed single-junction cells and also multijunction architectures.[1] Size-effect tuning also enables the use of inexpensive, abundant ultralow-band gap semiconductors otherwise unsuited for solar energy conversion.

Recently, colloidal quantum dot (CQD) solar cells were reported that reached above 5% Air Mass 1.5 (AM1.5) solar power conversion efficiencies.[2] These devices—known as depleted-heterojunction (DH)-CQD solar cells—took advantage of an N-p heterojunction between a transparent n-type TiO_2 electrode and an active layer consisting of PbS CQDs [Fig. 1(a)(i)]. The 1*S* electron excited state of the CQD lies well above (>0.3 eV) the TiO_2 conduction band level; photoexcited electron injection was favored therefore into TiO_2, both due to the band offset and the built-in potential from the N-p diode junction. The 1*P* hole level exhibits a large (>1.5 eV) discontinuity with the TiO_2 valence band, providing a sizeable barrier against the undesired passage of majority holes from the p-type CQD layer into the TiO_2 electrode. Holes were conducted away using a top Ohmic Au contact to the p-type PbS CQD layer.

DH-CQD photovoltaics overcame the limitations of prior work on Schottky barrier CQD devices[3,4] in three principal ways. First, the DH design employed a transparent electron-accepting TiO_2 contact, thereby benefiting more efficiently from minority carrier separation due to the placement of the junction on the illuminated side. Second, whereas the Schottky device's open-circuit voltage is limited by Fermi-level pinning due to defect states at the metal-semiconductor interface, the TiO_2-CQD interface benefited from passivation during the solution-phase deposition of the quantum dots. Third, a large discontinuity in the valence band of the DH device, combined with the minimization of electron density in the electron acceptor near the junction, maximized shunt resistance to enhance fill factor (FF) and minimized back-recombination to improve 1 sun performance.

As argued above, low cost is of primary interest in CQD solar cells; however, the use of an Au top contact raises questions regarding materials cost. The present manuscript

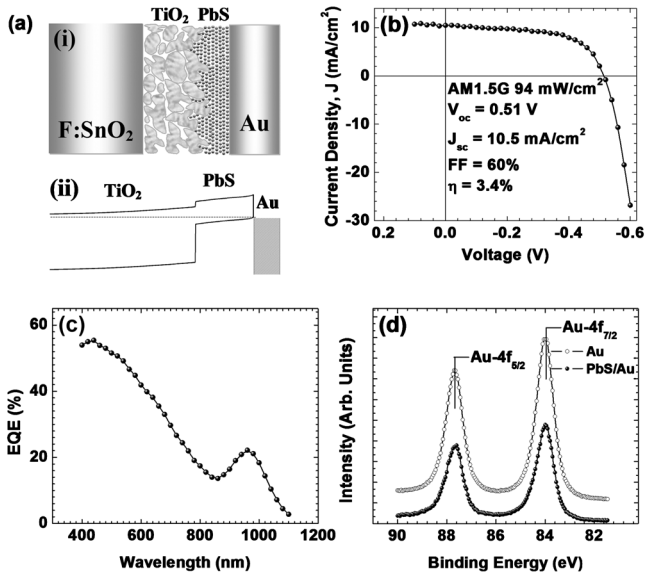

FIG. 1. (a) (i) The depleted heterojunction solar cell shows the transparent TiO_2 electrode and an active layer consisting of p-type PbS CQDs. Au provides the Ohmic contact on the PbS nanocrystal side. (ii) Spatial band alignment of TiO_2, PbS, and Au at equilibrium. The quasi Fermi energy is shown by the dotted line. (b) Current-voltage (J-V) response of a representative device from FTO-porous TiO_2–PbS–Au device. The device area is 0.049 cm^2. (c) EQE spectrum of the same device. (d) XPS data from pure Au and PbS–Au sample. The binding energies of Au $4f_{7/2}$ and Au $4f_{5/2}$ are located at 84.0 eV and 87.67 eV, respectively, for both the samples, indicating that no interfacial reaction takes place between PbS and Au.

a)Author to whom correspondence should be addressed. Electronic mail: ted.sargent@utoronto.ca.

TABLE I. Average performance of four representative devices made with each discussed metal contact. All data were obtained under 94 mW/cm^2 illumination (AM1.5).

Metal contact	J_{sc} (mA/cm^2)	V_{oc} (V)	FF (%)	Efficiency (%)
Au	10.7 ± 0.35	0.51 ± 0.01	57.7 ± 3	3.36 ± 0.1
Ni	0.8 ± 0.12	0.38 ± 0.05	43 ± 9	0.14 ± 0.03
LiF/Ni	10.1 ± 1.08	0.52 ± 0.02	58.1 ± 2	3.2 ± 0.34

seeks to address this limitation of past work by identifying a suitable top-contact to p-PbS CQD materials that can replace costly existing noble metals while achieving comparable efficiency.

For the purposes of the present study, we began by building a simple, nonoptimized version of Au-contacted cells which we could then adapt to the low-cost metallization strategy. We now briefly describe the fabrication and performance of these device platforms. We built our devices using layer-by-layer solution deposition of PbS CQDs capped with oleic acid (see the supplementary information for more details).[5] All film processing and device testing were carried out in air ambient. The control samples—depleted-heterojunction solar cells made using a Au electrode using the simplified baseline process—showed a short-circuit current density (J_{sc}) of 10.5 mA/cm^2, FF of 60%, and open-circuit voltage (V_{oc}) of 0.51 V corresponding to AM1.5 power conversion efficiency (η) of 3.4% [Fig. 1(b)]. In addition, the average performance of four representative devices made with Au electrode is also summarized in Table I. An external quantum efficiency (EQE) spectrum is provided in Fig. 1(c). When this curve is integrated with the standard AM1.5 spectrum, we calculate an expected J_{sc} of 13.5 mA/cm^2 which agrees well with our measured J_{sc}.

One attractive feature of using Au is that it provides a stable contact to the colloidal quantum dot film. As evidenced by x-ray photoelectron spectroscopy (XPS) [Fig. 1(d)], Au does not react with the PbS nanocrystals even though it is in direct physical and chemical contact with them.

Since, as explained above, cost considerations make it desirable to use alternative, lower-cost materials, we searched for metals having similar or deeper work functions with the goal of extracting holes from the quantum dot layer. From published work functions, platinum (Pt), palladium (Pd), selenium (Se), and nickel (Ni) should suffice.[6] However, Pt and Pd have the disadvantage of being very expensive noble metals and are not abundantly available on earth. Se is highly toxic.

This leaves abundant Ni as a good choice for Ohmic contact as it is inexpensive, relatively less toxic, and has been widely used as an electrode material in other common applications, such as batteries[7] and fuel cells.[8] Its silicide is used in microelectronics to contact complementary metal-oxide semiconductor integrated circuits because of its low resistivity, low temperature of formation, and good stability.[9]

Ni, however, has a more negative reduction potential (−0.25 V) than Pb (−0.13 eV).[6] As a consequence, one would expect that the PbS–Ni interface could reduce to a mixture of metallic Pb and nickel sulphide. We investigated whether this process indeed occured when Ni simply replaced Au as Ohmic metallization and, if so, whether it had a deleterious impact on performance.

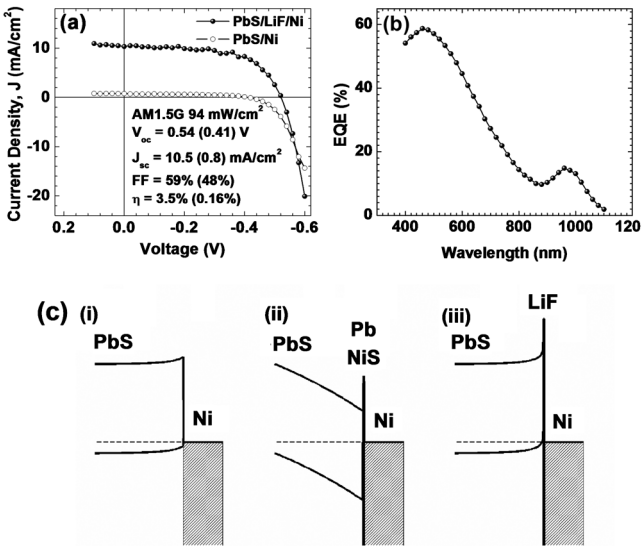

FIG. 2. (a) J-V response of devices made with and without LiF between PbS and Ni. (b) EQE spectrum of the devices made from LiF–Ni. The integrated J_{sc} (13.4 mA/cm^2) compares well with the J-V data. (c) Spatial band diagram at equilibrium of (i) PbS–Ni while assuming no interfacial reaction, i.e., sulfur interdiffusion, (ii) PbS–Pb/NiS–Ni, when sulfur interdiffusion takes place, and (iii) PbS–LiF–Ni when LiF acts as a thin tunnelling barrier and suppresses sulfur diffusion.

Ni-contacted devices showed very poor performance compared to Au, with J_{sc} of 0.8 mA/cm^2, FF of 48%, V_{oc} of 0.41 V, and η of 0.16% [Fig. 2(a)]. XPS data for the PbS–Ni interface indicated that the binding energy of Ni $2p_{3/2}$ increased to 853.0 eV due to the formation of nickel sulfide[10,11] as shown in Fig. 3(a). As seen in the Pb $4f$ spectrum, a metallic Pb signature at lower binding energy also emerges[12] [Fig. 3(c)]. As further evidence of nickel sulfide formation, the S $2p$ spectrum [Fig. 3(e)] indicates, when deconvolved, that both NiS and PbS species are present.

In sum, from XPS data, the chemical reaction between PbS and Ni results in the formation of nickel sulfide and metallic Pb at the interface. In principle, the work functions of the original PbS and Ni are suited to forming an Ohmic contact, but in practice, the formation of metallic Pb, with its shallow work function, establishes a Schottky junction between Pb and PbS, inhibiting hole injection into Ni [Fig. 2(c)(ii)], accounting for poor J-V performance [Fig. 2(a)].

We sought therefore to devise a contact strategy that would avoid interdiffusion among Ni and PbS. We would require a barrier to sulfur interdifussion that did not unduly impede hole extraction from the PbS to the Ni. Lithium fluoride (LiF) has given excellent results in organic photovoltaics, enhancing performance[13] and eliminating chemical reaction between the metal and the organic film[14] and nanocrystal.[15] We report the photovoltaic performance of a PbS–LiF–Ni device in Fig. 2(a).

The device with the interlayer performs as well as the Au-contacted control, achieving $J_{sc}=10.5$ mA/cm^2, FF $=59\%$, $V_{oc}=0.54$, and $\eta=3.5\%$ as shown in Fig. 2(a) (see also Table I). The corresponding EQE spectrum is shown in Fig. 2(b). XPS characterization of the PbS–LiF–Ni interface [Fig. 3(b)] reveals that the Ni $2p_{3/2}$ spectrum remains at 852.7 eV, indicating pure Ni-metal.[12] The Pb $4f$ spectrum reveals PbS with a lower level of PbO species [Fig. 3(d)]. No

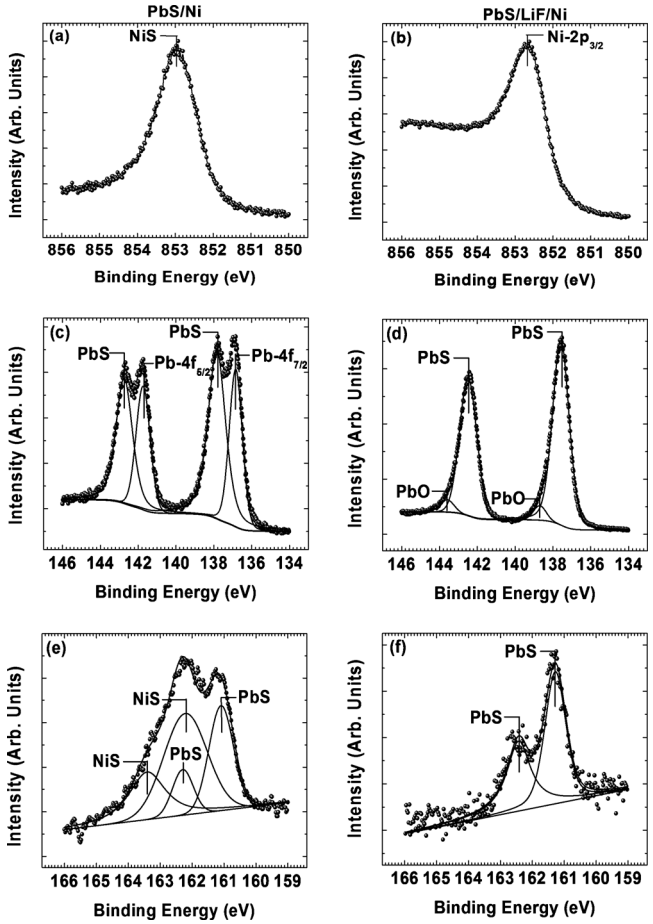

FIG. 3. XPS spectra from PbS–Ni (left) and PbS–LiF–Ni (right) interfaces. (a) and (b) Ni $2p_{3/2}$ spectra taken from pure Ni metal and compared with PbS–Ni and PbS–LiF–Ni samples. Without LiF, NiS is formed at the interface and Ni $2p$ peak moves to higher binding energy. A thin LiF layer prevents such a reaction. (c) and (d) PbS is reduced to Pb at the PbS–Ni interface, whereas LiF hinders such reduction for PbS–LiF–Ni devices. [(e) and (f)] Formation of NiS can also be seen from S $2p$ spectrum at the PbS–Ni interface. The existence of pure PbS is also confirmed for PbS–LiF–Ni devices.

metallic Pb is evident. The S $2p$ spectrum further confirms the presence of PbS alone [Fig. 3(f)]. While LiF is an insulator, it is present as such a thin layer between PbS and Ni that it does not unduly inhibit hole transport [Fig. 2(c)(iii)]. Instead, holes can tunnel through the LiF layer. This is consistent with our observation that further increasing the LiF thickness did reduce performance, with the series resistance and FF suffering first.

In conclusion, we have shown that DH-CQD solar cells using PbS nanocrystals and employing LiF–Ni as the top electrode achieve similar performance to device employing Au. XPS data indicate that when no LiF is inserted between PbS and Ni, metallic Pb and NiS accumulate at the interface, leading to poor device performance. The results offer promise along the path to realizing efficient, stable colloidal quantum dot photovoltaics.

R. Debnath would like to acknowledge the financial support through e8 scholarship. This publication was based on work supported in part by Award No. KUS-I1-009-21, made by King Abdullah University of Science and Technology (KAUST).

[1]E. H. Sargent, Nat. Photonics **3**, 325 (2009).
[2]A. G. Pattantyus-Abraham, I. J. Kramer, A. R. Barkhouse, X. Wang, G. Konstantatos, R. Debnath, L. Levina, I. Raabe, M. K. Nazeeruddin, M. Grätzel, and E. H. Sargent, ACS Nano **4**(6), 3374 (2010).
[3]K. W. Johnston, A. G. Pattantyus-Abraham, J. P. Clifford, S. H. Myrskog, D. D. MacNeil, L. Levina, and E. H. Sargent, Appl. Phys. Lett. **92**, 151115 (2008).
[4]G. I. Koleilat, L. Levina, H. Shukla, S. H. Myrskog, S. Hinds, A. G. Pattantyus-Abraham, and E. H. Sargent, ACS Nano **2**, 833 (2008).
[5]See supplementary material at http://dx.doi.org/10.1063/1.3463037 for more about nanocrystal synthesis, device fabrication, and testing.
[6]D. R. Lide, editor, *CRC Handbook of Chemistry and Physics*, 90th ed. (CRC, Boca Raton, FL, 2010).
[7]J. Hassoun, S. Panero, P. Simon, P. L. Taberna, and B. Scrosati, Adv. Mater. (Weinheim, Ger.) **19**, 1632 (2007).
[8]A. Le Goff, V. Artero, B. Jousselme, P. D. Tran, N. Guillet, R. Metaye, A. Fihri, S. Palacin, and M. Fontecave, Science **326**, 1384 (2009).
[9]C. Wyon, Eur. Phys. J.: Appl. Phys. **49**, 20101 (2010).
[10]S. Goh, A. Buckley, R. Lamb, W. Skinner, A. Pring, H. Wang, L.-J. Fan, L.-Y. Jang, L.-J. Lai, and Y.-w. Yang, Phys. Chem. Miner. **33**, 98 (2006).
[11]H. W. Nesbitt, D. Legrand, and G. M. Bancroft, Phys. Chem. Miner. **27**, 357 (2000).
[12]J. F. Moulder, W. F. Stickle, P. E. Sobol, and K. D. Bomben, *Handbook of X-ray Photoelectron Spectroscopy* (Perkin-Elmer, Eden Prairie, MN, 1992).
[13]C. J. Brabec, S. E. Shaheen, C. Winder, N. S. Sariciftci, and P. Denk, Appl. Phys. Lett. **80**, 1288 (2002).
[14]M. G. Mason, C. W. Tang, L. S. Hung, P. Raychaudhuri, J. Madathil, D. J. Giesen, L. Yan, Q. T. Le, Y. Gao, S. T. Lee, L. S. Liao, L. F. Cheng, W. R. Salaneck, D. A. dos Santos, and J. L. Bredas, J. Appl. Phys. **89**, 2756 (2001).
[15]J. Tang, X. Wang, L. Brzozowski, D. A. R. Barkhouse, R. Debnath, L. Levina, and E. H. Sargent, Adv. Mater. (Weinheim, Ger.) **22**, 1398 (2010).